STABILITY ANALYSIS OF THE INVERSE TRANSMEMBRANE POTENTIAL PROBLEM IN ELECTROCARDIOGRAPHY

MARTIN BURGER[1], BJØRN FREDRIK NIELSEN[2,3] AND KENT-ANDRÉ MARDAL[2,3]

[1]*Institute for Computational and Applied Mathematics,*
University of Münster,
Einsteinstrasse 62,
D-48149 Münster,
Germany

[2]*Simula Research Laboratory,*
P.O.Box 134,
1325 Lysaker,
Norway

[3]*Department of Informatics,*
P.O. Box 1080 Blindern,
0316 Oslo,
Norway

E-mail: martin.burger@wwu.de, bjornn@simula.no, kent-and@simula.no

ABSTRACT. In this paper we study some mathematical properties of an inverse problem arising in connection with electrocardiograms (ECGs). More specifically, we analyze the possibility for recovering the transmembrane potential in the heart from ECG recordings, a challenge currently investigated by a growing number of groups. Our approach is based on the bidomain model for the electrical activity in the myocardium, and leads to a parameter identification problem for elliptic partial differential equations (PDEs).

It turns out that this challenge can be split into two subproblems:
  (1) The task of recovering the potential at the heart surface from body surface recordings.
  (2) The problem of computing the potential inside the heart from the potential determined at the heart surface.
Problem (1), which can be formulated as the Cauchy problem for an elliptic PDE, has been extensively studied and is well-known to be severely ill-posed. The main purpose of this paper is to prove that problem (2) is stable and well-posed if a suitable prior is available. Moreover, our theoretical findings are illuminated by a series of numerical experiments. Finally, we discuss some aspects of uniqueness related to the anisotropy in the heart.

1. INTRODUCTION

The sources of the electrical voltages measured at the body surface in ECG recordings is the electrical pulses generated by the heart. This electrical activity is very important and closely linked to the blood pumping function of the myocardium. Many heart diseases lead to changes in the potential distribution and can therefore be identified by carefully examining ECG recordings.

The first human ECG was published by Augustus D. Waller in 1887. Since then it has become one of the most widespread and commonly used medical monitoring devices. This is probably due to the fact that heart conditions are among the most common diseases in the world [26] and the relatively low costs linked to buying and maintaining ECG machines.

In spite of its success, diagnoses based on manual inspection of ECGs often fail to detect heart diseases and malfunctions [3, 15, 27]. The outcome of such procedures is, of course, also highly depend upon the expertise and skills of the involved medical personnel. Thus, there is a need to improve this technology.

The purpose of this paper is to explore the possibilities for using mathematical models to compute the potential distribution within the heart from ECGs recorded at the body surface of a patient. If one manages to solve this problem, it could lead to the construction of new medical imaging devices providing the physicians with valuable information.

During the last three decades many researchers have analyzed inverse ECG problems, see e.g. [6, 10, 13, 8, 17, 18, 16, 19, 22, 23, 24, 31, 33, 34, 35, 38, 43, 44, 45, 46, 50]. In particular, the task of recovering the electrical potential at the heart surface, the so-called epicardial potential distribution, from body surface measurements has received a lot of attention. We will refer to this challenge as the *classical inverse ECG problem*. Note that the second formulation that could be called classical, namely the reconstruction

of epicardial activation sequences, is usually formulated into a linear inverse problem of exactly the same type. The purpose of such studies is to increase our knowledge about this organ. Furthermore, many diseases are revealed through changes in the epicardial potential. Nevertheless, mainly due to severe validation difficulties, it is still unclear when, or if, such techniques will come into clinical use, see chapters 7 and 8 in [24] and [39] for a discussion.

Mathematically, the classical inverse ECG problem leads to a Cauchy problem for a second order elliptic PDE. It has thus not only been thoroughly analyzed in the bioengineering literature, but also in classical mathematical texts [5, 9, 21] - to mention a few. More precisely, the potential at the heart surface is, even though it is uniquely identifiable, highly unstable with respect to uncertainties in the measured potential at the body surface. The reconstruction is a severely ill-posed problem and often approximately solved by invoking second order Tikhonov regularization. A simple introduction to the topic is presented in Chapter 7 in [48].

The aim of the present paper is to investigate whether this inverse solution process can be taken one step further. Namely, to analyze the task of computing the transmembrane potential <u>inside</u> the heart from the epicardial potentials generated by solving the classical problem. In fact, we will prove that this task can be formulated in terms of a stable set of equations, provided that proper topologies are used. On the other hand, the nullspace of the involved parameter-to-observation map contains nonzero elements. Consequently, in its original form, this problem does not have a unique solution. Apriori information about the potential distribution is hence needed in order to compute meaningful solutions. We analyze this problem both in terms of the closed range theorem and by considering it in view of the famous Babuška-Brezzi conditions for saddle point problems.

In [7] an "oblique dipole layer" model of the excitation wavefront inside the heart is proposed and analyzed. It contains interesting results regarding the unique identification of the wavefront from ECG data, i.e. information that might turn out to be important for understanding more about the nullspace of our parameter-to-observation map. However, please note that the present text mainly addresses stability issues and does not concern dipole layer models.

This paper is organized as follows: A brief presentation of the bidomain model is given in Section 2, sections 3 and 4 contain our stability analysis, and the numerical experiments are presented in Section 5. The nullspace associated with the inverse transmembrane potential problem is discussed in Section 6, and we summarize our findings in Section 7.

2. Bidomain model

The bidomain equations are widely accepted as an accurate model for the electrical activity in heart. They were developed during the 70s and 80s [36, 37, 51] and have been thoroughly studied by many scientists, see e.g. [25, 43, 48].

One may split the heart tissue into two parts; the intracellular and extracellular spaces separated by the cell membrane. In the bidomain modeling framework, each of these spaces are assigned a potential, i.e. the intracellular

potential u_i and the extracellular potential u_e. Furthermore, the myocardial tissue is regarded as a continuum medium[1] such that $u_i(x,t)$ and $u_e(x,t)$ are defined at every point x in the heart H and $t \in [0, t^*]$. Here, $[0, t^*]$ represents the time span of a heart beat.

By defining the transmembrane potential $v = u_i - u_e$, the scaled bidomain model take the form

$$
\text{(1)} \qquad \frac{\partial s}{\partial t} = F(s, v) \quad \text{for } x \in H,\, t \in [0, t^*],
$$

$$
\text{(2)} \qquad v_t + I(s, v) = \nabla \cdot (M_i \nabla v) + \nabla \cdot (M_i \nabla u_e) \quad \text{for } x \in H,\, t \in [0, t^*],
$$

$$
\text{(3)} \qquad \nabla \cdot (M_i \nabla v) + \nabla \cdot ((M_i + M_e) \nabla u_e) = 0 \quad \text{for } x \in H,\, t \in [0, t^*],
$$

where M_i and M_e are the intracellular and extracellular conductivity tensors, respectively, and F and I are given functions. The state vector $s = s(x, t)$ contains one to approximately fifty entries which represent gating variables and ionic currents. Details about (1)-(3) can be found in, e.g., [43, 48].

Equation (1) defines a system of ordinary differential equations at every point x in the heart. The form of this system depends on the vector function F used to incorporate the cell dynamics. Many such models have been proposed throughout the last three decades: Beeler and Reuter [2], DiFrancesco [11], Luo and Rudy [29, 30] and Winslow et al. [52], etc. The form of the total ionic current I is also determined by the particular framework used.

Let B denote the domain occupied by the entire body and define $T = B \setminus \overline{H}$, see Figure 1. Outside the heart there are no electrical sources and the involved tissues are passive conductors. The electrical potential u_o in T is thus governed by an elliptic PDE on the form:

$$
\text{(4)} \qquad \nabla \cdot (M_o \nabla u_o) = 0 \quad \text{for } x \in T,\, t \in [0, t^*],
$$

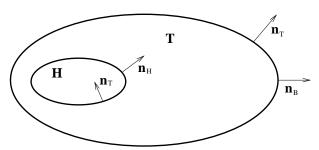where $M_o = M_o(x)$ is the conductivity in the torso T, cf. [48] for further details.

FIGURE 1. A schematic illustration of the domains and normal vectors involved in our study; the heart H, the torso T and the entire body $B = \overline{H} \cup T$. Note that $\mathbf{n_T} = -\mathbf{n_H}$ at ∂H and that $\partial T = \partial H \cup \partial B$.

We will assume that the surface ∂B of the body is electrically insulated, for example surrounded by air. This yields the boundary condition

$$
\text{(5)} \qquad (M_o \nabla u_o) \cdot \mathbf{n_B} = 0 \quad \text{on } \partial B,
$$

---

[1]Considering the intracellular space as a continuous volume is justified by the fact that cardiac cells are connected via so-called gap junctions. This topic is certainly beyond the scope of the present text. Further details can be found in [25, 43].

where $\mathbf{n_B}$ denotes the normal vector of ∂B of unit length. At the epicardial surface ∂H, separating the heart H from the torso T, one usually applies the interface condition

$$(6) \qquad\qquad u_e = u_o \quad \text{on } \partial H$$

for the potential, and

$$(7) \qquad\qquad (M_e \nabla u_e) \cdot \mathbf{n_H} = -(M_o \nabla u_o) \cdot \mathbf{n_T} \quad \text{on } \partial H,$$

$$(8) \qquad\qquad (M_i \nabla v + M_i \nabla u_e) \cdot \mathbf{n_H} = 0 \quad \text{on } \partial H,$$

for the currents. Here, $\mathbf{n_H}$ and $\mathbf{n_T}$ represent the outward normal vectors of ∂H and ∂T, respectively - see Figure 1. Equations (6) and (7) simply express that the extracellular potential and current are continuous at the heart surface. The property (8) is linked to the preservation of the total current. Further details about this topic can be found in [48]. Note that, adding (7) to (8) yields the equation

$$(9) \qquad ([M_i + M_e]\nabla u_e) \cdot \mathbf{n_H} + (M_i \nabla v) \cdot \mathbf{n_H} = -(M_o \nabla u_o) \cdot \mathbf{n_T} \quad \text{on } \partial H.$$

Provided that initial conditions for the transmembrane potential v and the state vector s are given, we can use (1)-(8) to simulate the electrical changes in the myocardium during one heart beat. This is a challenging scientific issue in itself, but not the topic of the present paper.

3. Inverse transmembrane potential problem

Let us now turn our attention toward the main purpose of this paper. That is, toward the task of computing the transmembrane potential inside the heart H from ECGs recorded at the body surface ∂B. As mentioned above, we might split this problem into two subtasks:

(1) Use the ECG to determine the potential at the heart surface ∂H.
(2) Use the result generated in (1) to compute v throughout H.

The next two subsections are devoted to each of these problems.

3.1. **Estimating the heart surface potential from ECG recordings.**
How can we use an ECG e recorded at the body surface ∂B to compute the epicardial potential? Combining the ECG with (4) and (5) yield (using standard notation for Sobolev spaces): Compute $u_o|_{\partial H} \in H^{1/2}(\partial H)$ from

$$(10) \qquad\qquad \nabla \cdot (M_o \nabla u_o) \;=\; 0 \quad \text{in } T,$$

$$(11) \qquad\qquad (M_o \nabla u_o) \cdot \mathbf{n_B} \;=\; 0 \quad \text{on } \partial B,$$

$$(12) \qquad\qquad u_o \;=\; e \quad \text{on } \partial B.$$

This is the classical Cauchy problem for second order elliptic PDEs, which has been extensively studied by many researchers, see e.g. [5, 9, 21]. Even though it is severely ill-posed, several regularization techniques have been constructed that seem to yield reconstructions of suitable quality by incorporating prior knowledge, e.g. second order Tikhonov regularization or the L_1-norm of the normal derivative (cf. [14]). Further details about this problem from an inverse ECG perspective can be found in the references cited in Section 1. Will not dwell any further upon the Cauchy problem, since it has already been thoroughly analyzed.

3.2. **Computing the Transmembrane Potential.** In the following we investigate the problem of computing the transmembrane potential from body surface potential maps. This problem can be decomposed into two steps, first of all the well-studied case of computing the epicardial potential from the data on the body surface, and secondly the extension into the heart to obtain the transmembrane potential. While the first part is known to be ill-posed with severe instability, we show that the second step is stable in a reasonable setting. The main issue in computing transmembrane potentials instead of epicardial potentials is the nullspace of the forward operator, which needs to be taken care of by prior knowledge - an issue we further discuss below.

In Section 3.2.1 we study this challenge in terms of the closed range theorem and in Section 3.2.2 by standard theory for saddle point problems. The former provides a rather compact analysis, whereas the latter yields a system of PDEs that can be solved to compute the transmembrane potential v throughout H.

3.2.1. *Analysis in terms of the closed range theorem.* In the following we provide an operator-theoretic analysis for the problem of computing the transmembrane potential from the epicardial potential. Let us start with the overall inverse problem of computing the transmembrane potential from measurements of the body surface, which can be formulated as the operator equation

$$(13) \qquad\qquad \mathcal{A}v = e,$$

where e are the potential recordings and $\mathcal{A}$ is the forward operator

$$(14) \qquad\qquad \mathcal{A} : H^1(H) \to L^2(\partial B), v \mapsto u_0|_{\partial B},$$

with u_0 connected to v via the forward model (3), (4), (5), (6), and (9) together with the normalization condition

$$(15) \qquad\qquad \int_{\partial H} u_0 \; d\sigma = 0.$$

Note that some normalization condition for the potential is always needed for the well-definedness of the forward model. We use (15) for simplicity, but alternative normalizations can be considered with analogous arguments.

We split the forward operator into

$$(16) \qquad\qquad \mathcal{A} = \mathcal{A}_2 \circ \mathcal{A}_1,$$

where $\mathcal{A}_2$ is the (standard) forward operator used for reconstructing the epicardial potential, i.e.

$$(17) \qquad\qquad \mathcal{A}_2 : H_\diamond^{1/2}(\partial H) \to L^2(\partial B), u|_{\partial H} \mapsto u_0|_{\partial B},$$

with u_0 satisfying (4)-(6), and $\mathcal{A}_1$ is the operator

$$(18) \qquad\qquad \mathcal{A}_1 : H^1(H) \to H_\diamond^{1/2}(\partial H), v \mapsto u_e|_{\partial H},$$

where u_0 and u_e satisfy the forward model (3), (4), (5), (6), (9), and (15).

Here $H_\diamond^{1/2}(\partial H)$ is defined via

$$(19) \qquad\qquad H_\diamond^{1/2}(\partial H) := \{h \in H^{1/2}(\partial H) \mid \int_{\partial H} h \; d\sigma = 0\}.$$

Our aim is to show that all ill-posedness (in the sense of instability) in the solution of (13) is included in the inversion of $\mathcal{A}_2$, while $\mathcal{A}_1$ is an operator with continuous generalized inverse but a possibly huge nullspace.

Theorem 3.1. *Let $\mathcal{A}_1$ be defined as above. Then*

$$(20) \qquad \mathcal{R}(\mathcal{A}_1) = H_\diamond^{1/2}(\partial H).$$

Proof. First of all, it is straight-forward to show that there exists a unique solution of (3), (4), (5), (6), (9), and (15). By the trace theorem it is clear that $\mathcal{R}(\mathcal{A}_1) \subset H^{1/2}(\partial H)$ and due to (15) $\mathcal{R}(\mathcal{A}_1)$ is indeed a subset of $H_\diamond^{1/2}(\partial H)$.

Vice versa, let $h \in H_\diamond^{1/2}(\partial H)$ be a function in $H^1(H)$ with trace h. Then there exists a unique solution u_0 of (4), (5), and

$$u_0 = h \qquad \text{on } \partial H.$$

Then the Neumann trace $M_0 \nabla u_0 \cdot \mathbf{n}_T$ is in $H^{-1/2}(\partial H)$ and has zero surface integral (from the solvability condition of the Neumann problem). Now let $u_e \in H^1(H)$ be an arbitrary function satisfying $u_e = h$ on ∂H. Then there exists a solution $v \in H^1(H)$ and $u_0 \in H^1(T)$ of the Neumann problem (3), (4), (5), (6), (9), since the solvability condition

$$\int_{\partial H} (([M_i + M_e]\nabla u_e) \cdot \mathbf{n_H} + (M_i \nabla v) \cdot \mathbf{n_H}) \, d\sigma = - \int_{\partial H} (M_o \nabla u_o) \cdot \mathbf{n_T} \, d\sigma = 0$$

holds. Hence, u_0, u_e, and v satisfy (3) - (6), (9), (15), which implies $h = \mathcal{A}_1 v$. $\qquad \square$

A particular consequence of the characterization of $\mathcal{R}(\mathcal{A}_1)$ is its closedness, since $H_\diamond^{1/2}(\partial H)$ is a Banach space (a subspace of co-dimension one in $H^{1/2}(\partial H)$). By the closed range theorem, this implies that the generalized inverse of $\mathcal{A}_1$ is a continuous linear operator.

We can further conclude that the operators $\mathcal{A}$ and $\mathcal{A}_2$ have related decay of singular values, more precisely there exist positive constants $\hat{c}_1$ and $\hat{c}_2$ such that

$$\hat{c}_1 \|A_2^* w\| \le \|A^* w\| \le \hat{c}_2 \|A_2^* w\|.$$

Indeed, $\hat{c}_1$ is the square of the smallest nonzero singular value of A_1 and $\hat{c}_2$ is the square of the largest singular value. From this relation it is possible to transfer stability estimates for the pseudo-inverse of $\mathcal{A}_2$, which are well-known in the literature (cf. [1]), to estimates of the pseudo-inverse of $\mathcal{A}$, with the same quantitative dependence on data error. This means that the reconstruction of the transmembrane potential is exactly as unstable as the reconstruction of the epicardial potential. We hence conclude that it makes sense to invert for the transmembrane potential if a good prior is available (needed to eliminate the nullspace).

3.2.2. *Analysis in terms of the Babuška-Brezzi conditions.* The purpose of this section is to explain how we may use data available at the heart surface to compute the transmembrane potential v throughout the entire heart wall. More specifically, we propose to do this by minimizing the deviation between v and a suitable prior subject to constraints given by equation (3) and boundary conditions on the epicardial surface ∂H.

Let us assume that we have managed to compute $d = u_o|_{\partial H} \in H^{1/2}(\partial H)$ and that we want to use this information to determine the transmembrane potential v inside the heart H. In principle, one could of course seek to use the bidomain model (1)-(3) in its full complexity to solve this problem. However, due to the involved steep gradients, the numerical solution of (1)-(3) is extremely CPU demanding [12, 42, 49] and consequently not well-suited for inverse solution procedures so far. Fortunately, as we will see below, it turns out to be possible to inversely compute v (from heart surface data) by only using equation (3).

Suppose that we have computed the heart surface potential $d = u_o|_{\partial H} \in H^{1/2}(\partial H)$ from an ECG recording e by solving the Cauchy problem (10)-(12). Our goal is to use d and

$$g = (M_o \nabla u_o) \cdot \mathbf{n_T} \quad \text{on } \partial H,$$

to compute v inside H, cf. (9). To this end, assume that some prior v_{prior} for the transmembrane potential throughout H is available[2]. In terms of mathematical symbols, our strategy can now be formulated as follows:

$$(21) \qquad \min_{v \in H^1(H)} \frac{1}{2} \|v - v_{\text{prior}}\|^2_{H^1(H)}$$

subject to the constraints

$$(22) \qquad \nabla \cdot [(M_i + M_e)\nabla u] + \nabla \cdot (M_i \nabla v) \;=\; 0 \quad \text{in } H,$$
$$(23) \qquad ([M_i + M_e]\nabla u) \cdot \mathbf{n_H} + (M_i \nabla v) \cdot \mathbf{n_H} \;=\; -g \quad \text{on } \partial H,$$
$$(24) \qquad \qquad \qquad \qquad \qquad Tu \;=\; d \quad \text{on } \partial H,$$

where $g \in H^{-1/2}(\partial H)$, $d \in H^{1/2}(\partial H)$, and

$$T : H^1(H) \to H^{1/2}(\partial H)$$

denotes the trace operator. For the sake of simple notation, we write u instead of u_e.

We will now use the Babuška-Brezzi theory for saddle point problems to analyze (21)-(24). More specifically, it turns out that this problem satisfies the inf-sup and coercivity conditions, provided that the conductivities M_i and M_e are well-behaved. This means that (21)-(24) defines a stable problem that can be solved by considering a system of PDEs. The details are as follows.

Assumptions. We will throughout this text assume that H is a Lipschitz domain, M_i and M_e are symmetric tensors, and that there exist positive constants c_1 and c_2 such that

$$(25) \qquad 0 < c_1 \leq \frac{\mathbf{a}^T M_i(x)\mathbf{a}}{\mathbf{a}^T \mathbf{a}} \leq c_2 \quad \text{for all } x \in H \text{ and all } \mathbf{a} \in \mathbb{R}^n \setminus \{0\},$$

$$(26) \qquad 0 < c_1 \leq \frac{\mathbf{a}^T M_e(x)\mathbf{a}}{\mathbf{a}^T \mathbf{a}} \leq c_2 \quad \text{for all } x \in H \text{ and all } \mathbf{a} \in \mathbb{R}^n \setminus \{0\},$$

where $n = 2$ or 3 depending on the spatial dimension of the problem under consideration.

---

[2]The availability of such a prior will be discussed below.

3.2.3. *Linear system.* The Lagrangian associated with (21)-(24) reads

$$L(v, u, w, q) = \frac{1}{2}\|v - v_{\text{prior}}\|^2_{H^1(H)} + (Tu - d, q)_{H^{1/2}(\partial H)}$$
$$+ \int_H (M_i + M_e)\nabla u \cdot \nabla w \, dx + \int_H M_i \nabla v \cdot \nabla w \, dx + \langle g, Tw \rangle$$

for $(v, u, w, q) \in H^1(H) \times H^1(H) \times W \times H^{1/2}(\partial H)$, where

$$W = \left\{ \psi \in H^1(H); \int_H \psi \, dx = 0 \right\}.$$

In a straightforward manner we find that the directional derivatives of L are

$$\langle \frac{\partial L}{\partial v}, \psi \rangle = (v - v_{\text{prior}}, \psi)_{H^1(H)} + \int_H M_i \nabla w \cdot \nabla \psi \, dx, \quad \psi \in H^1(H),$$

$$\langle \frac{\partial L}{\partial u}, \psi \rangle = \int_H (M_i + M_e)\nabla w \cdot \nabla \psi \, dx + (T\psi, q)_{H^{1/2}(\partial H)}, \quad \psi \in H^1(H),$$

$$\langle \frac{\partial L}{\partial w}, \psi \rangle = \int_H (M_i + M_e)\nabla u \cdot \nabla \psi \, dx + \int_H M_i \nabla v \cdot \nabla \psi \, dx + \langle g, T\psi \rangle, \quad \psi \in W,$$

$$\langle \frac{\partial L}{\partial q}, \psi \rangle = (Tu - d, \psi)_{H^{1/2}(\partial H)}, \quad \psi \in H^{1/2}(\partial H),$$

and the optimality condition

$$\frac{\partial L}{\partial v} = 0, \frac{\partial L}{\partial u} = 0, \frac{\partial L}{\partial w} = 0, \frac{\partial L}{\partial q} = 0$$

thus gives the following system: Find $v, u \in H^1(H)$, $w \in W$ and $q \in H^{1/2}(\partial H)$ such that

$$(27) \quad \begin{bmatrix} G & 0 & A'_i & 0 \\ 0 & 0 & A'_{i+e} & K' \\ A_i & A_{i+e} & 0 & 0 \\ 0 & K & 0 & 0 \end{bmatrix} \begin{bmatrix} v \\ u \\ w \\ q \end{bmatrix} = \begin{bmatrix} Gv_{\text{prior}} \\ 0 \\ -T^*g \\ Rd \end{bmatrix},$$

where

$$G : H^1(H) \to (H^1(H))', v \to (v, \cdot)_{H^1(H)},$$

$$A_i : H^1(H) \to (H^1(H))', v \to \int_H M_i \nabla v \cdot \nabla \cdot \, dx,$$

$$A_{i+e} : H^1(H) \to (H^1(H))', u \to \int_H (M_i + M_e)\nabla u \cdot \nabla \cdot \, dx,$$

$$K : H^1(H) \to (H^{1/2}(\partial H))', u \to (Tu, \cdot)_{H^{1/2}(\partial H)},$$

$$R : H^{1/2}(\partial H) \to (H^{1/2}(\partial H))', d \to (d, \cdot)_{H^{1/2}(\partial H)}.$$

Note that assumptions (25) and (26) imply that A_i and A_{i+e} define uniformly elliptic operators.

A solution of (21)-(24) is equivalently characterized by (27). We will therefore proceed by analyzing (27) and prove that this problem is well-posed.

Block system. Let us introduce the notation

$$X = H^1(H) \times H^1(H),$$
$$Y = W \times H^{1/2}(\partial H),$$
$$\|x\|_X = \left(\|x_1\|_{H^1(H)}^2 + \|x_2\|_{H^1(H)}^2 \right)^{1/2} \quad \text{for } x = (x_1, x_2) \in X,$$
$$\|y\|_Y = \left(\|y_1\|_{H^1(H)}^2 + \|y_2\|_{H^{1/2}(\partial H)}^2 \right)^{1/2} \quad \text{for } y = (y_1, y_2) \in Y.$$

By defining

(28) $$\mathbf{A} : X \to X', \ \mathbf{A} = \begin{bmatrix} G & 0 \\ 0 & 0 \end{bmatrix},$$

(29) $$\mathbf{B} : X \to Y', \ \mathbf{B} = \begin{bmatrix} A_i & A_{i+e} \\ 0 & K \end{bmatrix},$$

$$\mathbf{x} = (v, u)^T,$$
$$\mathbf{y} = (w, q)^T,$$

we may write (27) on the standard form: Find $x \in X$ and $y \in Y$ such that

(30) $$\begin{aligned} \mathbf{Ax} + \mathbf{B'y} &= [Gv_{\text{prior}} \ 0]^T \\ \mathbf{Bx} &= [-T^*g \ Rd]^T. \end{aligned}$$

Please note that

$$\langle \mathbf{A}x, y \rangle = (x_1, y_1)_{H^1(H)}$$

and

$$\begin{aligned} \langle \mathbf{B}x, y \rangle &= \int_H M_i \nabla x_1 \cdot \nabla y_1 \, dx \\ &+ \int_H (M_i + M_e) \nabla x_2 \cdot \nabla y_1 \, dx \\ &+ (Tx_2, y_2)_{H^{1/2}(\partial H)}. \end{aligned}$$

Coercivity. We will now prove that the operator $\mathbf{A}$ is coercive on the kernel

(31) $$Z = \{z \in X; \ \langle \mathbf{B}z, y \rangle = 0 \quad \text{for all } y \in Y\}$$

of $\mathbf{B}$.

Lemma 3.1. *There exists a positive constant c_3 such that the operator $\mathbf{A}$, defined in (28), satisfies*

$$\langle \mathbf{A}z, z \rangle \geq c_3 \|z\|_X^2 \quad \text{for all } z \in Z,$$

where $Z \subset X$ is the space defined in (31).

Proof. Let $z = (z_1, z_2) \in Z$ be arbitrary. Then $z \in Z$ implies that

$$\int_H M_i \nabla z_1 \cdot \nabla \psi \, dx + \int_H (M_i + M_e) \nabla z_2 \cdot \nabla \psi \, dx + (Tz_2, \phi)_{H^{1/2}(\partial H)} = 0$$

for all $\psi \in W$ and $\phi \in H^{1/2}(\partial H)$, and by choosing $\psi = z_2 - \int_H z_2 \, dx \in W$, $\phi = Tz_2 \in H^{1/2}(\partial H)$ we find that

(32) $$\int_H (M_i + M_e) \nabla z_2 \cdot \nabla z_2 \, dx + (Tz_2, Tz_2)_{H^{1/2}(\partial H)} = - \int_H M_i \nabla z_1 \cdot \nabla z_2 \, dx.$$

From (25) and the Cauchy-Schwarz inequality we conclude that

$$\int_H (M_i + M_e)\nabla z_2 \cdot \nabla z_2 \, dx + (Tz_2, Tz_2)_{H^{1/2}(\partial H)} \le c_2 \|z_1\|_{H^1(H)} \|z_2\|_{H^1(H)},$$

and (25)-(26) and Friedrich's inequality, see e.g. [32], imply that there exists a constant $c_5 > 0$ such that

$$c_5 \|z_2\|_{H^1(H)}^2 \le c_2 \|z_1\|_{H^1(H)} \|z_2\|_{H^1(H)}.$$

Consequently,

$$(33) \qquad \|z_2\|_{H^1(H)} \le c_6 \|z_1\|_{H^1(H)} \quad \text{for all } z = (z_1, z_2) \in Z,$$

where $c_6 = c_2/c_5$.

The coercivity of $\mathbf{A}$ on the nullspace Z of $\mathbf{B}$ follows easily from (33). More precisely, for any $z = (z_1, z_2) \in Z$:

$$
\begin{aligned}
\langle \mathbf{A}z, z \rangle &= \|z_1\|_{H^1(H)}^2 \\
&\ge \frac{1}{2}\|z_1\|_{H^1(H)}^2 + \frac{1}{2c_6^2}\|z_2\|_{H^1(H)}^2 \\
&= c_7(\|z_1\|_{H^1(H)}^2 + \|z_2\|_{H^1(H)}^2) \\
(34) \qquad &= c_7 \|z\|_X^2.
\end{aligned}
$$

$\square$

Inf-sup. Let us now show that the famous inf-sup condition holds.

Lemma 3.2. *There exists a positive constant c_4 such that the operator $\mathbf{B}$, defined in (29), satisfies*

$$\inf_{y \in Y} \sup_{x \in X} \frac{\langle \mathbf{B}x, y \rangle}{\|x\|_X \|y\|_Y} \ge c_4.$$

Proof. Let $y = (y_1, y_2) \in Y$ be arbitrary. Consider the harmonic extension $x_2 \in H^1(H)$ of $y_2 \in H^{1/2}(\partial H)$ to H, i.e x_2 satisfies

$$(35) \qquad \Delta x_2 = 0 \quad \text{in } H,$$
$$(36) \qquad Tx_2 = y_2 \quad \text{on } \partial H,$$

in the weak sense. Then there exists a constant c_8, only depending on the domain H, such that

$$(37) \qquad \|x_2\|_{H^1(H)} \le c_8 \|y_2\|_{H^{1/2}(\partial H)},$$

see e.g. [20]. Furthermore, let $x_1 \in H^1(H)$ denote the unique function satisfying[3]

$$
\begin{aligned}
(38) \qquad \int_H M_i \nabla x_1 \cdot \nabla \psi \, dx &= -\int_H (M_i + M_e)\nabla x_2 \cdot \nabla \psi \, dx \\
&\quad + (y_1, \psi)_{H^1(H)} \; \forall \psi \in H^1(H),
\end{aligned}
$$

$$(39) \qquad \int_H x_1 \, dx = 0.$$

---

[3](Note that by choosing $\psi = 1$ in (38) it follows that $\int_H y_1 \, dx = 0$, i.e. y_1 must belong to W).

By choosing $\psi = x_1$ in (38) and applying assumptions (25)-(26), the Cauchy-Schwarz and Poincaré's inequalities we conclude that

$$
\begin{aligned}
\|x_1\|_{H^1(H)} &\leq c_9 \left(\|x_2\|_{H^1(H)} + \|y_1\|_{H^1(H)} \right) \\
&\leq c_{10} \left(\|y_2\|_{H^{1/2}(\partial H)} + \|y_1\|_{H^1(H)} \right),
\end{aligned}
$$
(40)

where the last inequality follows from (37).

Define $\hat{x} = (x_1, x_2)$ where x_2 and x_1 denote the solutions of (35)-(36) and (38)-(39), respectively. By choosing $\psi = y_1$ in (38), and recalling that $Tx_2 = y_2$ along ∂H, it follows that

$$
\langle \mathbf{B}\hat{x}, y \rangle = (y_1, y_1)_{H^1(H)} + (y_2, y_2)_{H^{1/2}(\partial H} = \|y\|_Y^2.
$$

Moreover, (40) and (37) imply that

$$
\begin{aligned}
\|\hat{x}\|_X^2 &\leq c_{10}^2 \left(\|y_2\|_{H^{1/2}(\partial H)} + \|y_1\|_{H^1(H)} \right)^2 \\
&\quad + c_8^2 \|y_2\|_{H^{1/2}(\partial H)}^2 \\
&\leq c_{11}^2 \left(\|y_2\|_{H^{1/2}(\partial H)}^2 + \|y_1\|_{H^1(H)}^2 \right) \\
&= c_{11}^2 \|y\|_Y^2,
\end{aligned}
$$

and consequently

$$
\sup_{x \in X} \frac{\langle \mathbf{B}x, y \rangle}{\|x\|_X \|y\|_Y} \geq \frac{\langle \mathbf{B}\hat{x}, y \rangle}{\|\hat{x}\|_X \|y\|_Y} = \frac{\|y\|_Y^2}{\|\hat{x}\|_X \|y\|_Y} \geq \frac{\|y\|_Y^2}{c_{11} \|y\|_Y \|y\|_Y} = \frac{1}{c_{11}},
$$

Finally, since y was arbitrary, we conclude that

$$
\inf_{y \in Y} \sup_{x \in X} \frac{\langle \mathbf{B}x, y \rangle}{\|x\|_X \|y\|_Y} \geq \frac{1}{c_{11}}.
$$

$\square$

By applying straightforward techniques, one can show that $\mathbf{A}; X \to X'$ and $\mathbf{B} : X \to Y'$ are continuous. Consequently, standard theory for saddle point problems imply that (see e.g. [4]):

Theorem 3.2. *The operator*

$$
\mathcal{A} : X \times Y \to X' \times Y', \ \mathcal{A} = \begin{bmatrix} \mathbf{A} & \mathbf{B}' \\ \mathbf{B} & 0 \end{bmatrix}
$$

is continuously invertible. Here, $\mathbf{A}$ and $\mathbf{B}$ are the mappings defined in (28) and (29), respectively.

By combining Theorem 3.2 with the analysis presented above we conclude that; for every $v_{\text{prior}} \in H^1(H)$, the problem (21)-(24) has a unique solution $v \in H^1(H)$ which depends continuously on the data $(d, g) \in (H^{1/2}(\partial H, H^{-1/2}(\partial H))$. That is, (21)-(24) is well-posed, and the solution of this problem can be computed by solving the system (27).

4. Heart models with cavities

So far we have ignored the cavities in the heart. We will now briefly discuss this issue by reconsidering the coercivity and inf-sup conditions presented in lemmas 3.1 and 3.2.

Let $C = CL \cup CR$, where CL and CR are the domains occupied by the left and right heart cavities, see Figure 2. Note that the transmembrane potential v only is defined in the heart wall H, whereas the state equation is defined in both H and C. The model (21)-(24) must thus be changed accordingly:

$$(41) \qquad \min_{v \in H^1(H)} \frac{1}{2} \|v - v_{\text{prior}}\|^2_{H^1(H)}$$

subject to

$$(42) \qquad \nabla \cdot (M \nabla u) = \begin{cases} -\nabla \cdot (M_i \nabla v) & \text{in } H, \\ 0 & \text{in } C, \end{cases}$$

$$(43) \qquad ([M_i + M_e] \nabla u) \cdot \mathbf{n_H} + (M_i \nabla v) \cdot \mathbf{n_H} = -g \quad \text{on } \partial H,$$

$$(44) \qquad Tu = d \quad \text{on } \partial H,$$

$$(45) \qquad u_e = u_C \quad \text{on } \partial C$$

$$(46) \qquad (M_e \nabla u_e) \cdot \mathbf{n_H} = -(M_C \nabla u_C) \cdot \mathbf{n_C} \quad \text{on } \partial C,$$

$$(47) \qquad (M_i \nabla v + M_i \nabla u_e) \cdot \mathbf{n_H} = 0 \quad \text{on } \partial C,$$

where $u_e = u|_H$, $u_C = u|_C$ and $\mathbf{n_C}$ is the outward directed normal vector of unit length of ∂C. Note that the interface conditions (45)-(47) on ∂C are similar to those valid at the epicardial surface, cf. (6)-(8). Since the cavities are filled with blood, the function M takes the form

$$(48) \qquad M(x) = \begin{cases} M_i(x) + M_e(x) & \text{for } x \in H, \\ M_C & \text{for } x \in C. \end{cases}$$

where M_C is the conductivity of blood. Recall that $g \in H^{-1/2}(\partial H)$ and $d \in H^{1/2}(\partial H)$ are given data.

The solution u of the state equation (42) is harmonic in C. This fact plays an important role in our analysis, and we therefore introduce the Hilbert space

$$(49) \qquad Q = \left\{ \psi \in H^1(H \cup C) | \int_C \nabla \psi \cdot \nabla \phi \, dx = 0 \text{ for all } \phi \in H^1_0(C) \right\}.$$

For the present model, the corresponding Lagrangian, cf. sections 3.2.2 and 3.2.3, thus reads

$$\begin{aligned} L(v, u, w, q) &= \frac{1}{2} \|v - v_{\text{prior}}\|^2_{H^1(H)} \\ &+ \int_{H \cup C} (M \nabla u) \cdot \nabla w \, dx + \int_H M_i \nabla v \cdot \nabla w \, dx + \langle g, Tw \rangle \\ &+ (Tu - d, q)_{H^{1/2}(\partial H)} \end{aligned}$$

for $(v, u, w, q) \in H^1(H) \times Q \times W \times H^{1/2}(\partial H)$, where

$$W = \left\{ \psi \in Q | \int_H \psi \, dx = 0 \right\}.$$

With cavities the Hilbert spaces associated with the saddle point problem are

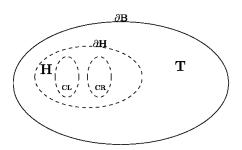$$X = H^1(H) \times Q,$$
$$Y = W \times H^{1/2}(\partial H).$$

FIGURE 2. Torso T, heart wall H, and cavities CL and CR. In this text we employ the notation $C = CL \cup CR$ and $\partial C = \partial CL \cup \partial CR$. Note that ∂H denotes the epicardium, <u>not</u> including the endocardial surfaces ∂CL and ∂CR.

The proof of Lemma 3.1 (coercivity) is based on proving inequality (33). For the present model, this is achieved as follows. Analogous to (32), we find that

$$(50) \quad \int_{H \cup C} (M \nabla z_2) \cdot \nabla z_2 \, dx + (T z_2, T z_2)_{H^{1/2}(\partial H)} = - \int_H M_i \nabla z_1 \cdot \nabla z_2 \, dx,$$

and the Cauchy-Schwarz inequality implies that

$$\int_{H \cup C} (M \nabla z_2) \cdot \nabla z_2 \, dx + (T z_2, T z_2)_{H^{1/2}(\partial H)} \le c_{12} \|z_1\|_{H^1(H)} \|z_2\|_{H^1(H)}.$$

Since the epicardial surface ∂H constitutes the boundary of $H \cup C$, we may employ Friedrich's inequality to conclude that there exists a constant $c_{13} > 0$ such that

$$c_{13} \|z_2\|^2_{H^1(H \cup C)} \le c_{12} \|z_1\|_{H^1(H)} \|z_2\|_{H^1(H)} \le c_{12} \|z_1\|_{H^1(H)} \|z_2\|_{H^1(H \cup C)}.$$

Consequently,

$$(51) \qquad\qquad \|z_2\|_{H^1(H \cup C)} \le c_{14} \|z_1\|_{H^1(H)},$$

where $c_{14} = c_{12}/c_{13}$. The coercivity on the kernel of the state equation is now a simple consequence of (51), cf. (34).

Next, we consider the inf-sup condition. Let $\psi \in Q$ be arbitrary, where Q is defined in (49). Since ψ is harmonic in the cavities C, it follows from standard stability results for elliptic PDEs that there exists a constant c_{15}, independent of ψ, such that

$$\|\psi\|_{H^1(C)} \le c_{15} \|\psi\|_{H^{1/2}(\partial C)} \le c_{15} (\|\psi\|_{H^{1/2}(\partial C)} + \|\psi\|_{H^{1/2}(\partial H)}).$$

From the trace theorem we thus conclude that

$$(52) \qquad \|\psi\|_{H^1(C)} \le c_{16}\|\psi\|_{H^1(H)} \quad \text{for all } \psi \in Q.$$

We can employ (52) to generalize the argument for the inf-sup condition, presented in the proof of Lemma 3.2, to the present situation. The details are as follows.

For arbitrary $y = (y_1, y_2) \in Y$, let $x_2 \in H^1(H)$ be the unique solution of

$$(53) \qquad \Delta x_2 = 0 \quad \text{in } H \cup C,$$
$$(54) \qquad Tx_2 = y_2 \quad \text{on } \partial H.$$

Classical stability estimates imply that there exists a constant c_{17} such that

$$(55) \qquad \|x_2\|_{H^1(H \cup C)} \le c_{17}\|y_2\|_{H^{1/2}(\partial H)}.$$

Clearly, $C \subset H \cup C$ and therefore $x_2 \in Q$.

Next, consider the bilinear form

$$a(\psi, \phi) = \int_H M_i \nabla\phi \cdot \nabla\psi \, dx \quad \text{for } \phi, \psi \in W.$$

From Poincaré's inequality we find that

$$a(\phi, \phi) \ge c_{18}\|\phi\|^2_{H^1(H)} \quad \text{for all } \phi \in W,$$

and since $W \subset Q$ inequality (52) implies that

$$a(\phi, \phi) \ge c_{19}\|\phi\|^2_{H^1(H \cup C)} \quad \text{for all } \phi \in W.$$

We conclude that $a(\cdot, \cdot)$ is coercive on $W \times W$. The continuity of $a(\cdot, \cdot)$ is verified by employing straightforward techniques.

The linear functional

$$l(\psi) = -\int_{H \cup C} M \nabla x_2 \cdot \nabla\psi \, dx + (y_1, \psi)_{H^1(H \cup C)} \quad \text{for } \psi \in W$$

is bounded. From Riesz Representation Theorem we thus conclude that there exists a unique element $r \in W$ satisfying

$$a(r, \psi) = l(\psi) \quad \text{for all } \psi \in W.$$

If we choose x_1 to be the restriction of r to H, then $x_1 \in H^1(H)$ and by invoking standard estimates for elliptic PDEs one finds that

$$\begin{aligned}
\|x_1\|_{H^1(H)} &\le \|r\|_{H^1(H \cup C)} \\
&\le c_{20}\left(\|x_2\|_{H^1(H \cup C)} + \|y_1\|_{H^1(H \cup C)}\right) \\
&\le c_{21}\left(\|y_2\|_{H^{1/2}(\partial H)} + \|y_1\|_{H^1(H \cup C)}\right),
\end{aligned}$$

where the last inequality follows from (55). The remaining part of the proof of the inf-sup condition for heart models with cavities is analogous to the argument presented in connection with Lemma 3.2.

5. NUMERICAL EXPERIMENTS

We now turn our attention toward an experimental study of the theoretical findings presented above. The tests will be performed on 2D heart models with cavities, see Figure 2, and only address the problem of computing the transmembrane potential from heart surface potentials. The task of determining the voltages at the heart surface from body surface data can, as briefly discussed above, be handled by solving a standard Cauchy problem for an elliptic PDE.

5.1. **Software issues.** In order to ease the implementation of software for solving (41)-(47) we remove the inhomogeneous Dirichlet condition (44) by using a harmonic extension $\bar{d}$ of $d \in H^{1/2}(\partial H)$ to $H^1(H \cup C)$. More specifically, $\bar{d} \in H^1(H \cup C)$ is the unique solution of

$$(56) \qquad\qquad \Delta \bar{d} \;=\; 0 \quad \text{in } H \cup C,$$

$$(57) \qquad\qquad T\bar{d} \;=\; d \quad \text{on } \partial H,$$

and we define

$$\bar{u} = u - \bar{d}.$$

In addition, a simple penalty method, parameterized by $0 < \epsilon \ll 1$ is invoked such that the transmembrane potential v can be extended to be defined in both the heart wall H and in the cavities C. We thus suggest the following penalized approximation of (41)-(47):

$$(58) \qquad \min_{v \in H^1(H)} \left\{ \frac{1}{2}\|v - v_{\text{prior}}\|^2_{H^1(H)} + \epsilon\frac{1}{2}\|v - v_{\text{prior}}\|^2_{H^1(C)} \right\}$$

subject to the constraints

$$(59) \qquad \nabla \cdot [M\nabla \bar{u}] = \begin{cases} -\nabla \cdot (M_i \nabla v) - \nabla \cdot \left[M\nabla \bar{d}\right] & \text{in } H, \\ -\epsilon \nabla \cdot (M_i \nabla v) - \nabla \cdot \left[M\nabla \bar{d}\right] & \text{in } C, \end{cases}$$

$$(60) \qquad (M\nabla \bar{u}) \cdot \mathbf{n_H} + (M_i \nabla v) \cdot \mathbf{n_H} = -(M\nabla \bar{d}) \cdot \mathbf{n_H} - g \quad \text{on } \partial H,$$

$$(61) \qquad T\bar{u} = 0 \quad \text{on } \partial H,$$

where we, for the sake of convenience, have omitted to repeat the interface conditions on the boundary ∂C of the heart cavities, cf. (45)-(47). Furthermore, the intracellular conductivity M_i is extrapolated to also be defined in C, and M is defined in (48).

Our procedure for computing the transmembrane potential v from the heart surface data d and g, cf. the third paragraph of Section 3.2.2, hence consists of two steps:

- Determine the harmonic extension $\bar{d}$ of d by solving (56)-(57).
- Solve the optimality system associated with (58)-(61) with the finite element method. (For further details about how to derive such optimality systems, please see Section 3.2.3).

Concerning the size of the penalty parameter ϵ, we used $\epsilon = 10^{-4}$ in all the examples presented below. Simulations with smaller values for ϵ produced virtually the same results.

5.2. **Prior.** If the heart surface quantities g and d are available, one can in principle compute the transmembrane potential v at any time during a heart beat by solving (58)-(61). However, a suitable prior is needed in order to obtain meaningful results. This is a delicate issue and, as far as the authors know, reasonable priors are not available at arbitrary time instances. In the numerical experiments we will therefore focus on the resting phase of the heart cycle and ischemic heart disease.

Ischemia is a reversible precursor of heart infarction caused by partial occlusion of one or more of the arteries/vessels supplying blood to the heart. Consequently, there might be subregions, referred to as ischemic regions, in the organ not receiving sufficient blood. If the condition persists, this may eventually lead to an infarction.

According to reported lab measurements [28], the transmembrane potential v has a particularly simple structure during the resting phase. More specifically, v is constant in both the healthy tissue and in the ischemic region(s) with a transition zone in-between. Figure 3 shows the resting transmembrane potential computed by solving the bidomain model (1)-(3) with altered cell dynamics in the ischemic zone, see e.g. [47] for further details. Motivated by this information, we considered the reconstruction of v during rest, employed the prior $v_{\mathrm{prior}} = -96mV$, and checked whether the ischemic location could be identified.
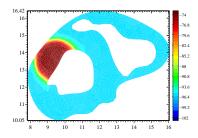

FIGURE 3. The resting transmembrane potential v generated by solving the bidomain model with modified cell properties in the ischemic region.

5.3. **Examples.** We considered five different test cases. In each case we added uniformly distributed noise N to the true heart surface potential d and two measures for the noise level were used:

- Mean amplitude:

$$(62) \qquad \frac{\frac{1}{n}\sum_{i=1}^{n}|N(i)|}{\max d - \min d},$$

   where n denotes the number of mesh points at the heart surface.
- Relative L_2:

$$(63) \qquad \sqrt{\frac{\int_{\partial\Omega}|N|^2 ds}{\int_{\partial\Omega}|d - d_{mean}|^2 ds}},$$

   where d_{mean} is the mean value of d.

Notice that the mean value of N was zero in all the experiments. We use both measures, since in the mathematical literature it is more common to define the noise level in the relative L_2 sense, whereas in the biomedical literature one refers to amplitudes when defining the amount of noise in ECG signals.

Please note that <u>no regularization</u> was used in the reconstructions presented below.

5.3.1. *Test 1: Transmural posterior ischemia.* Figure 4 shows the results obtained for a transmural posterior ischemia. The ischemic region can easily be identified with 53 % noise, measured in the relative L_2 sense, in the data. However, the size of the ischemic zone is underestimated and the method fails to identify the transmural property of the true lesion. In view of our theoretical findings, we find it reasonable to suspect that these shortcomings are caused by our choice of prior.

5.3.2. *Test 2: Transmural anterior ischemia.* The results shown in Figure 5 for a transmural anterior ischemia are similar to those observed in Test 1. This indicates that anterior and posterior transmural lesions are approximately equally difficult to identify - at least if heart surface data is used in the reconstruction process.

5.3.3. *Test 3: Subendocardial anterior ischemia.* We also explored whether subendocardial lesions could be recovered. Results concerning such a case are shown in Figure 6. Even though the reconstructions are of lower quality than those obtained for the transmural cases in Test 1 and Test 2, it is still possible to roughly identify the position of the ischemic region with 49 % noise (relative L_2) in the heart surface potential d.

5.3.4. *Test 4: Ischemia in the septum.* The identification of ischemia in the region between the cavities is more challenging than the examples explored in tests 1-3, see Figure 7. Nevertheless, please note that the largest values of the reconstructed transmembrane potentials occur in the septum, not far away from the true ischemic region. Moreover, the reconstruction obtained with 40 % noise (relative L_2) is almost as good as the one computed with no noise.

5.3.5. *Test 5: A healthy heart.* Noisy data didn't introduce any false ischemic regions in the tests with a healthy heart shown in Figure 8. In this case the noise free heart surface potential d was constant, consequently $\max d - \min d = 0$, and the noise measures defined in (62)-(63) couldn't be used. We have therefore instead included the range of the uniformly distributed noise N in Figure 8.

6. Nullspace and Specific Priors

Since we have shown above that the computation of the transmembrane potential given the epicardial potential is a stable problem, we now discuss the remaining issue, namely the nullspace in the map between the transmembrane and epicardial potential.

6.1. **Monodomain Case.** We start with the simple case of proportional anisotropies, i.e.

$$(64) \qquad\qquad M_e(x) = \lambda M_i(x) \qquad x \in H$$

for some positive constant λ, where the bidomain model actually reduces to the monodomain case. Under this condition it is well-known that u_e can be explicitly computed from (3)

$$\nabla \cdot (M_i \nabla((1 + \lambda)u_e + v)) = 0$$

as

$$(65) \qquad\qquad u_e(x) = -\frac{1}{1 + \lambda} v(x)$$

If the support of v is a compact subset of H all (Neumann and Dirichlet) boundary values of u_e on ∂H vanish. In particular ischemic regions cannot be seen at all from electrical measurements.

A similar reasoning holds for almost proportional conductivities, which we model by an expansion of the form

$$(66) \qquad\qquad M_e(x) = \lambda M_i(x) + \epsilon \tilde{M}_e \qquad x \in H$$

with ϵ small. Then we look for u_e in an expansion of the form

$$(67) \qquad\qquad u_e(x) = u_e^0(x) + \epsilon u_e^1(x) + \mathcal{O}(\epsilon^2).$$

It is straight-forward to see that the correct asymptotic yields again

$$u_e^0(x) = -\frac{1}{1 + \lambda} v(x),$$

hence u_e^0 does not contribute to the boundary data if v has compact support. The next order is determined from the elliptic equation

$$\nabla \cdot ((1 + \lambda)M_i \nabla u_e^1 - \frac{1}{1 + \lambda}\tilde{M}_e \nabla v)) = 0,$$

which yields a solution u_e^1 not proportional to v if $\tilde{M}_e$ is not proportional to M_i, and hence potentially nonzero contribution to the boundary data. Even if the contribution is nonzero, we observe that u_e is at most of order ϵ at the boundary, and hence also u_0 will be of order ϵ at the boundary of ∂B. For small values of ϵ this nonzero part will definitely be dominated by measurement noise and it again becomes impossible to reconstruct a transmembrane potential under practical conditions.

6.2. **Piecewise Constant Shapes.** A particularly interesting prior knowledge is an approximately piecewise constant shape of the transmembrane potential, e.g. during the resting phase of the heart, where the transmembrane potential is known to approximately have two specific values in healthy respectively ischemic tissue. In the following we will hence further study the potential identifiability or non-identifiability of piecewise constant transmembrane potentials with only two pre-determined values. For the simplicity of notation we assume that the scaling of the potential is such that

$$(68) \qquad\qquad v(x) = \chi_\Omega(x) = \begin{cases} 1 & x \in \Omega \\ 0 & x \in H \setminus \Omega, \end{cases}$$

where Ω is the ischemic subregion of the heart. This means that the ECG is scaled such that the healthy heart yields potential recordings zero. We shall assume that Ω is a disjoint union of a finite number of domains with C^1-boundaries, whose closure lies entirely in H. Moreover we assume that $H \setminus \Omega$ is simply connected.

As we shall see below the identifiability depends heavily on the anisotropies in M_i and M_e and their directions relative to the orientation $\partial\Omega$. In the oversimplified case of isotropic conductivities the ischemic regions remain completely invisible to electrical data.

Due to the low regularity of v in a piecewise constant model, we need to resort to very weak formulations of (3). If u, v satisfy (3), then for all functions $\varphi \in C_0^\infty(H)$, the equality

(69)
$$\int_H \nabla \cdot ((M_i + M_e)\nabla\varphi)u \ dx = -\int_H \nabla \cdot (M_i\nabla\varphi)v \ dx = -\int_\Omega \nabla \cdot (M_i\nabla\varphi) \ dx.$$

Applying Gauss' Theorem we have

$$\int_H \nabla \cdot ((M_i + M_e)\nabla\varphi)u \ dx = -\int_{\partial\Omega} (M_i\nabla\varphi) \cdot n \ d\sigma.$$

By choosing test functions φ supported in the interior of Ω or $H \setminus \Omega$ respectively, it is straight-forward to see that u solves

(70)
$$\nabla \cdot ((M_i + M_e)\nabla u) = 0 \qquad \text{in } H \setminus \partial\Omega,$$

since $\nabla v \equiv 0$ in $H \setminus \partial\Omega$. It hence remains to derive appropriate interface conditions on $\partial\Omega$. For this sake we split (69) into integrals on $H \setminus \Omega$ and Ω and integrate by parts. Denoting by n the exterior normal vector and by $[\psi]$ the jump of a quantity ψ across $\partial\Omega$ (limit from $H \setminus \overline{\Omega}$ minus limit from Ω)

$$\begin{aligned}
\int_H \nabla \cdot ((M_i + M_e)\nabla\varphi)u \ dx &= -\int_{H\setminus\partial\Omega} ((M_i + M_e)\nabla\varphi) \cdot \nabla u \ dx \\
&\quad -\int_{\partial\Omega} [(M_i + M_e)\nabla\varphi)u] \cdot \sigma \\
&= \int_{H\setminus\partial\Omega} \nabla \cdot ((M_i + M_e)\nabla u)\varphi \ dx \\
&\quad -\int_{\partial\Omega} [(M_i + M_e)\nabla\varphi)u] \cdot n \ d\sigma \\
&\quad +\int_{\partial\Omega} [(M_i + M_e)\nabla u)\varphi] \cdot n \ d\sigma.
\end{aligned}$$

Due to (70) the first term vanishes and noticing that with the assumed smoothness of test functions φ and $\nabla\varphi$ are continuous across $\partial\Omega$, we conclude from (69)

(71)
$$\int_{\partial\Omega} (((M_i + M_e)[\nabla u]) \cdot n\varphi - ((M_i + M_e)\nabla\varphi) \cdot n[u] + (M_i\nabla\varphi) \cdot n) \ d\sigma = 0$$

We finally mention that due to the density of C^∞ in C^1, (71) actually holds for all test functions $\varphi \in C^1(U)$, where U is an open set such that $\partial\Omega \subset U$ and $\overline{U} \subset \Omega$.

6.3. **Non-Proportional Anisotropies.** In the following we further examine the case of non-proportional anisotropies, for simplicity restricting ourself to spatial dimension two with spatially constant tensors M_i and M_e. In principle a similar treatment seems possible in spatial dimension three, but then the differential geometry of the surfaces becomes more involved, which shadows the main arguments.

We shall assume that M_i and M_e are both positive definite, but not proportional by a scalar factor. It is easy to check that this condition can be written equivalently as

$$(72) \qquad \frac{\lambda_1(M_i + M_e)}{\lambda_2(M_i + M_e)} > \frac{\lambda_1(M_i)}{\lambda_2(M_i)},$$

where $\lambda_1(M)$ denotes the largest and λ_2 the smallest eigenvalue of M.

The general intuition, confirmed by numerical results in [40, 41], is that ischemic regions can be well detected from body surface potential measurements for realistic anisotropies. In particular such regions should lead to boundary measurements different from the healthy heart. Such a general statement is difficult to prove, but here we provide at least a partial result for a class of subregions, showing that indeed there is a significant set of ischemic regions that result into nonzero body surface potential maps, and hence the situation completely differs from the one with proportional anisotropies.

Proposition 6.1. *Let $\partial\Omega$ be of class C^2 and include a straight part (curvature zero) with positive one-dimensional Hausdorff measure. Then for each $\Gamma \subset \partial B$ with positive measure we have $u_0|_\Gamma \neq 0$.*

Proof. Assume $u_0 \equiv 0$ on $\Gamma \subset \partial B$ with Γ having nonzero boundary measure. By the uniqueness of the Cauchy problem for elliptic equations we conclude $u_0 \equiv 0$ in $B \setminus H$. As a consequence $u_0 \equiv 0$ and $\nabla u_0 \equiv 0$ on ∂H. The interface conditions on ∂H further imply $u \equiv 0$ and $\nabla u \equiv 0$ on ∂H. Using (70) we can again conclude $u \equiv 0$ in $H \setminus \Omega$ by the uniqueness of the Cauchy problem. Hence, all jump terms in (71) are just the one-sided limits from inside Ω, i.e. we have

$$\int_{\partial\Omega} \left((-(M_i + M_e)\nabla u) \cdot n\varphi + ((M_i + M_e)\nabla\varphi) \cdot nu + (M_i\nabla\varphi) \cdot n \right) \, d\sigma = 0.$$

In the following let

$$a := ((M_i + M_e)n) \cdot n, \quad b := ((M_i + M_e)n) \cdot \mathtt{t} \quad c := (M_i n) \cdot n, \quad d := (M_i n) \cdot \mathtt{t},$$

where $\mathtt{t}$ is the tangent vector on $\partial\Omega$. Then the interface condition can be rewritten as

$$\int_{\partial\Omega} \left(-a\frac{\partial u}{\partial n}\varphi - b\frac{\partial u}{\partial\sigma}\varphi + a\frac{\partial\varphi}{\partial n}u + b\frac{\partial\varphi}{\partial\sigma}u + c\frac{\partial\varphi}{\partial n} + d\frac{\partial\varphi}{\partial\sigma} \right) \, d\sigma = 0.$$

Now let φ be a test function such that $\phi \equiv 0$ on $\partial\Omega$, then also $\frac{\partial\varphi}{\partial\sigma} \equiv 0$ and hence,

$$\int_{\partial\Omega} \left(a\frac{\partial\varphi}{\partial n}u + c\frac{\partial\varphi}{\partial n} \right) \, d\sigma = 0.$$

Since $\frac{\partial \varphi}{\partial n}$ can still be chosen arbitrarily, we conclude

$$u = -\frac{c}{a} \qquad \text{on } \partial\Omega.$$

Taking a test function with vanishing normal derivative, but arbitrary on $\partial\Omega$ we have after integration by parts with respect to σ we conclude

$$\int_{\partial\Omega} \left(a\frac{\partial u}{\partial n}\varphi + b\frac{\partial u}{\partial \sigma}\varphi + \varphi\frac{\partial(bu)}{\partial \sigma} + \varphi\frac{\partial d}{\partial \sigma} \right) \, d\sigma = 0.$$

From the arbitrary choice of φ we conclude

$$a\frac{\partial u}{\partial n} = -b\frac{\partial u}{\partial \sigma} - \frac{\partial(bu)}{\partial \sigma} - \frac{\partial d}{\partial \sigma}.$$

Now assume there exists a straight subset Σ of $\partial\Omega$ with positive measure. Since n and $\mathbf{t}$ are constant on Σ, we conclude that a, b, c, and d are constant on Σ. Hence, $\frac{\partial u}{\partial n} = 0$ and $u = -\frac{c}{a}$ is constant. By the uniqueness of the Cauchy problem for (70) we conclude that u is constant in the connected component Ω_0 of Ω to whose boundary Γ belongs. This implies that $\frac{\partial u}{\partial n} = 0$ on $\partial\Omega_0$, i.e. from the above formula for the normal derivative

$$b\frac{\partial u}{\partial \sigma} + \frac{\partial(bu)}{\partial \sigma} + \frac{\partial d}{\partial \sigma} = 0.$$

Inserting $u = -\frac{c}{a}$ we further conclude

$$0 = -2\frac{b}{a}\frac{\partial c}{\partial \sigma} + 2\frac{bc}{a^2}\frac{\partial a}{\partial \sigma} - \frac{c}{a}\frac{\partial b}{\partial \sigma} - \frac{\partial d}{\partial \sigma}$$

From the Frenet formulas in the plane we conclude

$$\frac{\partial a}{\partial \sigma} = -2b\kappa, \quad \frac{\partial c}{\partial \sigma} = -2d\kappa$$

and

$$\frac{\partial b}{\partial \sigma} = (a - \mathbf{t} \cdot ((M_i + M_e)\mathbf{t}))\kappa, \quad \frac{\partial d}{\partial \sigma} = (c - \mathbf{t} \cdot (M_i\mathbf{t}))\kappa.$$

Hence, in each part of $\partial\Omega_0$ with nonzero curvature we conclude

$$4\frac{bd}{a} - 4\frac{b^2c}{a} + \frac{c}{a}\mathbf{t} \cdot ((M_i + M_e)\mathbf{t})) - \mathbf{t} \cdot (M_i\mathbf{t}) = 0.$$

Since $\partial\Omega_0$ is a closed curve there exists a point $x_0 \in \partial\Omega_0$ such that $\mathbf{t}$ is an eigenvector of (M_i+M_e) corresponding to the larger eigenvalue $\lambda_1(M_i+M_e)$, and consequently also n is the eigenvector of the second eigenvalue. Then

$$b(x_0) = ((M_i + M_e)n) \cdot \mathbf{t} = \lambda n \cdot \mathbf{t} = 0.$$

Now we can choose such an x_0 with the further property that there exists $x_0^\delta \in \partial\Omega_0$ in a ball of radius δ around x_0 such that the curvature at x_0^δ is nonzero. In particular the remainder terms

$$r = 4\frac{bd}{a} - 4\frac{b^2c}{a}$$

satisfy $r(x_0^\delta) \to 0$ as $\delta \to 0$, since $a(x_0^\delta)$ is uniformly positive and $b(x_0) = 0$. Hence, the equality

$$r(x_0^\delta) + \frac{c(x_0^\delta)}{a(x_0^\delta)}\mathbf{t}(x_0^\delta) \cdot ((M_i + M_e)\mathbf{t}(x_0^\delta)) - \mathbf{t}(x_0^\delta) \cdot (M_i\mathbf{t}(x_0^\delta)) = 0$$

implies in the limit $\delta \to 0$

$$\frac{c(x_0)}{a(x_0)} \mathtt{t}(x_0) \cdot ((M_i + M_e)\mathtt{t}(x_0)) - \mathtt{t}(x_0) \cdot (M_i\mathtt{t}(x_0))$$

respectively after inserting c and a

$$\frac{\lambda_1(M_i + M_e)}{\lambda_2(M_i + M_e)} = \frac{\mathtt{t} \cdot ((M_i + M_e)\mathtt{t})}{n \cdot ((M_i + M_e)n)} = \frac{\mathtt{t} \cdot (M_i\mathtt{t})}{n \cdot (M_in)} \leq \frac{\lambda_1(M_i)}{\lambda_2(M_i)},$$

which contradicts our original assumption. $\square$

Note that the assumption of the ischemic region having a straight part is mainly a technical one. The first part of the proof is a general derivation and it would remain to discuss the compatibility condition for an elliptic Cauchy problem with boundary data

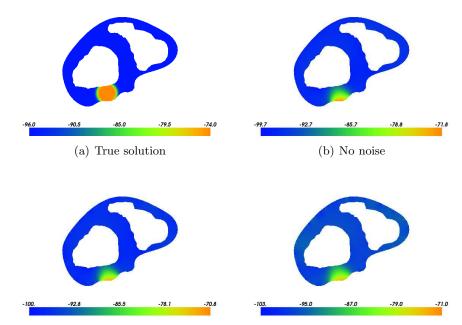$$u = -\frac{c}{a} \qquad \text{on } \partial\Omega$$

and

$$a\frac{\partial u}{\partial n} = -b\frac{\partial u}{\partial \sigma} - \frac{\partial(bu)}{\partial \sigma} - \frac{\partial d}{\partial \sigma} \qquad \text{on } \partial\Omega.$$

This is of course easier in the case with straight part, where u is constant and $\frac{\partial u}{\partial n}$ vanishes.

Our preliminary result might be just the starting point of a more detailed study of the dependence of the inversion on the anisotropic structure of the heart. A particularly important question in this respect is to characterize ischemia that can or cannot be uniquely reconstructed from body surface potential measurements. As mentioned in the Introduction, the results presented in [7] might turn out to be important for achieving this goal. We hope to be able to stimulate future research on this topic.
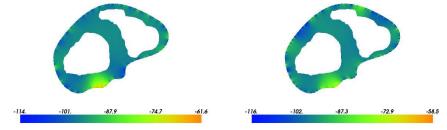
7. SUMMARY AND CONCLUSIONS

Most research addressing inverse problems arising in connection with ECG data focus on the computation of epicardial voltage distributions or activation sequences. We have investigated whether such inverse solutions can be taken one step further. More precisely, we have analyzed the task of computing the transmembrane potential inside the heart from heart surface data. In our main result we showed that this problem can be formulated in terms of a stable set of partial differential equations, provided that proper topologies are employed. Unfortunately, the solution of the problem is not unique, and consequently, the reconstruction of transmembrane voltages inside the myocardium must be guided by additional medical information.

During the resting phase of the heart cycle the transmembrane potential is known to be approximately constant in a healthy heart. This information can be used to define a suitable prior for identifying voltage changes due to ischemic heart disease. In a number of test cases this approach was used to explore our theoretical findings by performing numerical experiments with synthetic data. As predicted by our mathematical analysis, these computations turned out to be robust with respect to noise in the input data - no regularization was needed. On the other hand, these tests also revealed the importance of having a good prior, which turned out to be particularly important for identifying ischemia in the region between the left and right

(a) True solution

(b) No noise

(c) 28% relative L_2 noise, 5% mean ampli- (d) 53% relative L_2 noise, 10% mean am-
tude noise   plitude noise

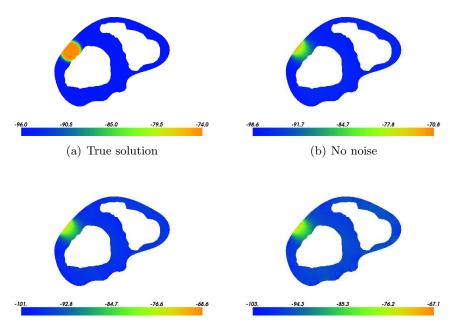(e) 140% relative L_2 noise, 26% mean am- (f) 211% relative L_2 noise, 40% mean am-
plitude noise   plitude noise

FIGURE 4. The first case concerns a transmural posterior
ischemia. The true solution is shown in the uppermost left
panel. The uppermost panel to the right shows the result
obtained with noise free data. The remaining figures were
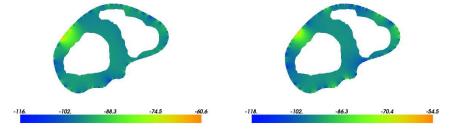computed with varying degree of noise.

ventricles. Further apriori knowledge should therefore be invoked and tests
with clinical data must be undertaken.

REFERENCES

[1] G. Alessandrini and E. Sincich. Detecting nonlinear corrosion by electrostatic mea-
    surements. *Applicable Analysis*, 85:107–128, 2006.
[2] G. W. Beeler and H. Reuter. Reconstruction of the action potential of ventricular
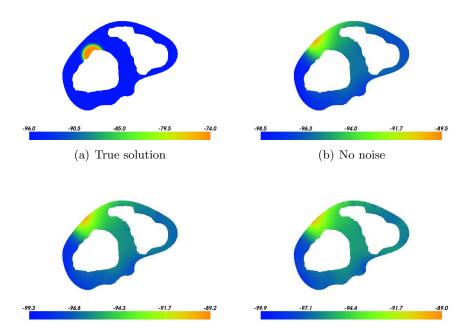   myocardial fibres. *Journal of Physiology*, 268:177–210, 1977.

(a) True solution

(b) No noise

(c) 28% relative L_2 noise, 5% mean amplitude noise

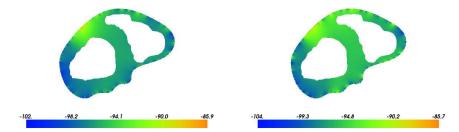(d) 57% relative L_2 noise, 10% mean amplitude noise

(e) 148% relative L_2 noise, 26% mean amplitude noise

(f) 212% relative L_2 noise, 37% mean amplitude noise

FIGURE 5. The second case concerns a transmural anterior ischemia. The true solution is shown in the uppermost left panel. The uppermost panel to the right shows the result obtained with noise free data. The remaining figures were computed with varying degree of noise.

[3] Y Birnbaum and B. J. Drew. The electrocardiogram in ST elevation acute myocardial infarction: correlation with coronary anatomy and prognosis. *Postgrad. Med. J.*, 79, 2003.

[4] D. Braess. *Finite elements. Theory, fast solvers, and applications in solid mechanics.* Cambridge University Press, second edition, 2001.

[5] A. Calderon. Uniqueness in the cauchy problem for partial differential equations. *American Journal of Mathematics*, 80:16–36, 1958.

[6] L. K. Cheng, J. M. Bodely, and J. Pullan. Comparison of potential- and activation-based formulations for the inverse problem of electrocardiology. *IEEE Transactions on Biomedical Engineering*, 50(1):11–22, January 2003.
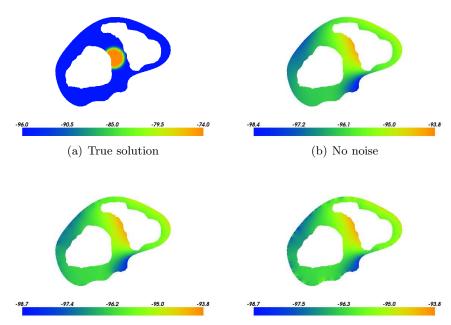
(a) True solution

(b) No noise

(c) 26% relative L_2 noise, 5% mean ampli- (d) 49% relative L_2 noise, 10% mean am-
tude noise   plitude noise
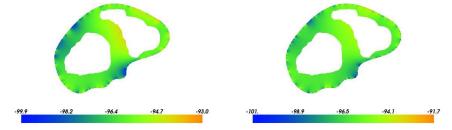
(e) 132% relative L_2 noise, 26% mean am- (f) 189% relative L_2 noise, 38% mean am-
plitude noise   plitude noise

FIGURE 6. The third case concerns a subendocardial anterior
ischemia. The true solution is shown in the uppermost left
panel. The uppermost panel to the right shows the result
obtained with noise free data. The remaining figures were
computed with varying degree of noise.

[7] P. Colli Franzone, L. Guerri, and E. Magenes. Oblique dipole layer potentials for
    direct and inverse problems of electrocardiology. *Mathematical Biosciences*, 68:23–
    55, 1984.
[8] P. Colli Franzone, L. Guerri, S. Tentonia, C. Viganotti, and S. Baruffi. A mathe-
    matical procedure for solving the inverse potential problem of electrocardiography:
    Analysis of the time-space accuracy from in vitro experimental data. *Mathematical
    Biosciences*, 77:353–396, 1985.
[9] R. Courant and D. Hilbert. *Methods of Mathematical Physics*, volume II. John Wiley
    & Sons, 1962.

(a) True solution

(b) No noise

(c) 20% relative L_2 noise, 5% mean ampli- (d) 40% relative L_2 noise, 10% mean am-
tude noise   plitude noise

(e) 104% relative L_2 noise, 26% mean am- (f) 145% relative L_2 noise, 36% mean am-
plitude noise   plitude noise

FIGURE 7. The fourth case concerns an ischemic region in
the septum. The true solution is shown in the uppermost left
panel. The uppermost panel to the right shows the result
obtained with noise free data. The remaining figures were
computed with varying degree of noise.

[10] J. Cuppen and A. van Oosterom. Model studies with inversly calculated isochrones
     of ventricular depolarization. *IEEE Transactions on Biomedical Engineering*, BME-
     31:652–659, 1984.

[11] D. DiFrancesco and D. Noble. A model of cardiac electrical activity incoporating
     ionic pumps and concentration changes. *Philosophical Transactions of the Royal So-
     ciety of London. Series B, Biological Sciences*, 307:353–398, 1985.

[12] R. Weber dos Santos, G. Plank, S. Bauer, and E. Vigmond. Parallel multigrid pre-
     conditioner for the cardiac bidomain model. *IEEE Transactions on Biomedical Engi-
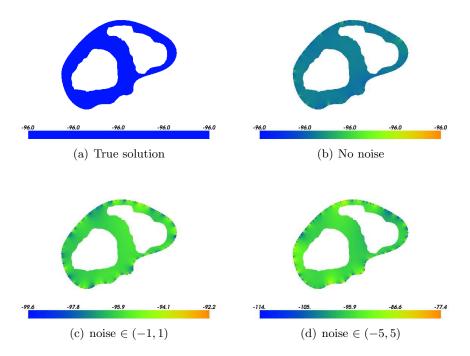   neering*, 51:1960–1968, 2004.

FIGURE 8. The fifth case concerns a healthy heart. The uppermost panel to the right shows the result obtained with noise free data. The remaining two figures were computed with varying degree of noise.

[13] O. Dössel. Inverse problem of electro- and magnetocardiography: Review and recent progress. *International Journal of Bioelectromagnetism*, 2(2), 2000.

[14] S. Ghosh and Y. Rudy. Application of L1-norm regularization to epicardial potential solution of the inverse electrocardiography problem. *Annals of Biomedical Engineering*, 37:902–912, 2009.

[15] P.H. Ginn, B. Jamieson, and M.D. Mendoza. Clinical inquiries. How accurate is the use of ECGs in the diagnosis of myocardial infarct? *The Journal of Family Practice*, 55:539–40, 2006.

[16] F. Greensite. Second-order approximation of the pseudoinverse for operator deconvolutions and families of ill-posed problems. *SIAM J. Appl. Math.*, 59(1):1–16, 1998.

[17] F. Greensite. Myocardial activation imaging. In P. Johnston, editor, *Computational inverse problems in electrocardiography*, pages 143–190. WIT Press, 2001.

[18] F. Greensite and G. Huiskamp. An improved method for estimating epicardial potentials from the body surface. *IEEE Transactions on Biomedical Engineering*, 45(1):98–104, January 1998.

[19] R. M. Gulrajani. Forward and inverse problems of electrocardiography. *IEEE Engineering in Medicine and Biology*, 17(5):84–101, September 1998.

[20] W. Hackbusch. *Elliptic Differential Equations. Theory and Numerical Treatment*. Springer-Verlag, 1992.

[21] L. Hörmander. *Linear Partial Differential Operators*. Springer-Verlag, 1976.

[22] G. Huiskamp and F. Greensite. A new method for myocardial activation imaging. *IEEE Transactions on Biomedical Engineering*, 44(6):433–446, 1997.

[23] G. Huiskamp and A. van Oosterom. The depolarization sequence of the human heart surface computed from measured body surface potentials. *IEEE Transactions on Biomedical Engineering*, 35:1047–1058, 1988.

[24] P. Johnston, editor. *Computational Inverse Problems in Electrocardiography*. WIT Press, 2001.

[25] J. Keener and J. Sneyd. *Mathematical Physiology*. Springer-Verlag, 1998.

[26] H.C. Kung, D.L. Hoyert, J.Q. Xu, and S.L. Murphy. Final data for 2005. National vital statistics reports. Technical Report vol 56 no 10, National Center for Health Statistics, 2005.

[27] J. Lau, J. P. Ioannidis, E. M Balk, C. Milch, N. Terrin, P. W. Chew, and D. Salem. Diagnosing acute cardiac ischemia in the emergency department: a systematic review of the accuracy and clinical effect of current technologies. *Ann. Emerg. Med.*, 37:453–460, 2001.

[28] D. Li, C. Y. Li, A. C. Yong, and D. Kilpatrick. Source of electrocardiographic ST changes in subendocardial ischemia. *Circulation Research*, 82:957–970, 1998.

[29] C. H. Luo and Y. Rudy. A model of the ventricular cardiac action potential: Depolarisation, repolarisation, and their interaction. *Circulation Research*, 68:1501–1526, 1991.

[30] C. H. Luo and Y. Rudy. A dynamic model of the cardiac ventricular action potenial. *Circulation Research*, 74:1071–1096, 1994.

[31] R. S. MacLeod and D. H. Brooks. Recent progress in inverse problems in electrocardiology. *IEEE Engineering in Medicine and Biology*, 17(1):73–83, January 1998.

[32] J. T. Marti. *Introduction to Sobolev Spaces and Finite Element Solution of Elliptic Boundary Value Problems*. Academic Press, 1986.

[33] B. J. Messinger-Rapport and Y. Rudy. The inverse problem in electrocardiography: A model study of the effects of geometry and conductivity parameters on the reconstruction of epicardial potentials. *IEEE Transactions on Biomedical Engineering*, 33:667–676, 1986.

[34] B. Messnarz, M. Seger, R. Modre, G. Fischer, F. Hanser, and B. Tilg. A comparison of noninvasive reconstruction of epicardial versus transmembrane potentials in consideration of the null space. *IEEE Transactions on Biomedical Engineering*, 51(9):1609–1618, 2004.

[35] B. Messnarz, B. Tilg, R. Modre, G. Fischer, and F. Hanser. A new spatiotemporal regularization approach for reconstruction of cardiac transmembrane potential patterns. *IEEE Transactions on Biomedical Engineering*, 51(2):273–281, 2004.

[36] W. T. Miller and D. B. Geselowitz. Simulation studies of the electrocardiogram I. the normal heart. *Circ. Res*, 43(2):301–315, 1978.

[37] W. T. Miller and D. B. Geselowitz. A bidomain model for anisotropic cardiac muscle. *Ann Biomed. Eng*, 11:191–206, 1983.

[38] R. Modre, B. Tilg, G. Fischer, and P. Wach. Noninvasive myocardial activation time imaging: a novel inverse algorithm applied to clinical ECG mapping data. *IEEE Transactions on Biomedical Engineering*, 49(10):1153–1161, 2002.

[39] M. P. Nash and A. J. Pullan. Challenges facing validation of noninvasive electrical imaging of the heart. *The Annals of Noninvasive Electrocardiology*, 10(1):73–82, 2005.

[40] B. F. Nielsen, X. Cai, and O. M. Lysaker. On the possibility for computing the transmembrane potential in the heart with a one shot method; an inverse problem. *Mathematical Biosciences*, 210(2):523–553, 2007.

[41] B. F. Nielsen, O. M. Lysaker, P. Grøttum K. A. Mardal, A. Tveito, C. Tarrou, K. Haugaa, A. Abildgaard, and J. G. Fjeld. Can ECG recordings and mathematics tell the condition of your heart? In A. Tveito, A. M. Bruaset, and O. Lysne, editors, *Simula Research Laboratory - by thinking constantly about it*, chapter 22, pages 287–319. Springer, Heidelberg, 2009.

[42] G. Plank, M. Liebmann, R. Weber dos Santos, E. J. Vigmond, and G. Haase. Algebraic multigrid preconditioner for the cardiac bidomain model. *IEEE Transactions on Biomedical Engineering*, 54:585–596, 2007.

[43] A. J. Pullan, M. L. Buist, and L. K. Cheng. *Mathematically Modelling the Electrical Activity of the Heart: From Cell to Body Surface and Back*. World Scientific Publishing Company, 2005.

[44] A. J. Pullan, L. K. Cheng, M. P. Nash, C. P. Bradley, and D. J. Paterson. Noninvasive electrical imaging of the heart: Theory and model development. *Annals of Biomedical Engineering*, 29(10):817–836, 2001.

[45] Y. Rudy and B. J. Messinger-Rapport. The inverse problem in electrocardiography: Solutions in terms of epicardial potentials. *Critical Reviews in Biomedical Engineering*, 16:215–268, 1988.

[46] Y. Rudy and H. S. Oster. The electrocardiographic inverse problem. *Critical Reviews in Biomedical Engineering*, 20:25–45, 1992.

[47] Tomas Syrstad Ruud, Bjørn Fredrik Nielsen, Ola Marius Lysaker, and Joakim Sundnes. A computationally efficient method for determining the size and location of myocardial ischemia. *IEEE Transactions on Biomedical Engineering*, 56(2):263–272, 2009.

[48] J. Sundnes, G. T. Lines, X. Cai, B. F. Nielsen, K. A. Mardal, and A. Tveito. *Computing the Electrial Activity in the Heart*. Springer-Verlag, 2006.

[49] J. Sundnes, B. F. Nielsen, K. A. Mardal, X. Cai, G. T. Lines, and A. Tveito. On the computational complexity of the bidomain and the monodomain models of electrophysiology. *Annals of Biomedical Engineering*, 34(7):1088–1097, 2006.

[50] B. Tilg, G. Fischer, R. Modre, F. Hanser, B. Messnarz, M. Schocke, C. Kremser, T. Berger, F. Hintringer, and F. X. Roithinger. Model-based imaging of cardiac electrical excitation in humans. *IEEE Transactions on Medical Imaging*, 21(9):1031–1039, 2002.

[51] L. Tung. *A Bidomain model for describing ischemic myocardial D-C potentials*. PhD thesis, MIT, Cambridge, MA, 1978.

[52] R. L. Winslow, J. Rice, S. Jafri, E. Marban, and B. O'Rourke. Mechanisms of altered excitation-contraction coupling in canine tachycardia-induced heart failure, II, model studies. *Circulation Research*, 84:571–586, 1999.